

Transferring Information Across Medical Images of Different Modalities

Jakub Nalepa^{1,2}, Piotr Mokry¹, Janusz Szymanek¹ and Michael P. Hayball^{1,3,4}

¹*Future Processing, Gliwice, Poland*

²*Silesian University of Technology, Gliwice, Poland*

³*Feedback PLC, Cambridge, U.K.*

⁴*Cambridge Computed Imaging, Cambridge, U.K.*

Keywords: Multimodal Analysis, ROI Transfer, DICOM.

Abstract: Multimodal analysis plays a pivotal role in medical imaging and has been recognized as an established tool in clinical diagnosis. This joint investigation allows for extracting various bits of information from images of different modalities, which can complement each other to provide a comprehensive view to the patient case. Since those images may be acquired using different protocols, their synchronization and transferring information, e.g., regions of interest (ROIs) between them is not trivial. In this paper, we derive the formulas for mapping ROIs between different modalities and show a real-life PET/CT example of such image processing.

1 INTRODUCTION

Multimodal image information is useful not only for visualization, analysis and interpretation of the images, but also for undertaking multicenter clinical consultations which allow for improving patient care by designing better therapy and follow-up strategies. Therefore, such approaches become common practice in clinical and pre-clinical imaging, and they are a very active research topic worldwide. In practical scenarios, combining the *structural* (anatomical) information with the *functional* information is of the biggest value. The ultimate goal of multimodal imaging is to maximize the diagnostic (and very often prognostic for several combinations (Greulich and Sechtem, 2015)) value of differently acquired images which may not be fully exploited otherwise.

There are numerous approaches for multimodal analysis that couple different image modalities in both side-by-side and fusion modes (Greulich and Sechtem, 2015). In the latter techniques, the images require further processing—they need to be registered, due to potential misplacement caused by patient breathing or motion (Deregnacourt et al., 2016). Clinical cases have shown that single-photon emission computed tomography/computed tomography (SPECT/CT) and positron emission tomography/computed tomography (PET/CT) are the established diagnostic tools for radiologists (Pichler et al., 2008). An important downside of CT imaging is a significant radiation

dose that affects the patient, and the limited soft tissue contrast provided by CT. Therefore, coupling magnetic resonance imaging (MRI) with PET (in PET/MRI systems) is being intensively developed—such systems can deliver morphologic, functional and molecular information simultaneously (Estorch and Carrio, 2013; Vandenberghe and Marsden, 2015). The current challenges in the multimodal imaging have been summarized in several surveys and reviews (Estorch and Carrio, 2013; Martí-Bonmatí et al., 2010; Sui et al., 2012).

In this paper, we focus on the side-by-side analysis of multimodal images. We derive formulas for transferring information between images, using only the acquisition protocol information available in DICOM (**D**igital **I**maging and **C**ommunications in **M**edicine), being a standard for exchanging medical image data. The formulas can be easily applied to images of any modalities in order to transfer annotated regions of interests (ROIs) between them. This ROI transfer is very useful in techniques for automated segmentation and analysis of multimodal medical images—as already mentioned, the structural information can be enhanced by the functional information in search of various tissues of interest (Nalepa et al., 2016).

Section 2 defines the prerequisites which are used in Section 3 to derive formulas utilized for transferring ROIs across different modalities. In Sect. 4, we show a real-life example of transferring information between PET and CT. Section 5 concludes the paper.

2 DEFINITIONS AND USEFUL EQUALITIES

Section 3—they will be exploited to retrieve the equations for mapping ROIs between images of different modalities.

In this section, we gather the prerequisites, and derive and prove useful equalities that will become handy in

Definition 1. Consider the following orthonormal vectors:

$$\vec{F}_1 = (F_{11}, F_{21}, F_{31}) \text{ and } \vec{F}_2 = (F_{12}, F_{22}, F_{32})$$

where

$$\begin{aligned} & |\vec{F}_1| = 1, |\vec{F}_2| = 1 \quad \Rightarrow \\ \Rightarrow & F_{11}^2 + F_{21}^2 + F_{31}^2 = F_{12}^2 + F_{22}^2 + F_{32}^2 = 1 \end{aligned} \quad (1)$$

$$\vec{F}_1 \circ \vec{F}_2 = F_{11}F_{12} + F_{21}F_{22} + F_{31}F_{32} = 0 \quad (2)$$

Additionally, let us introduce

$$\vec{n} = (n_1, n_2, n_3) = \vec{F}_1 \times \vec{F}_2. \quad (3)$$

Expanding Eq. 3, we obtain:

$$\vec{n} = \begin{bmatrix} n_1 \\ n_2 \\ n_3 \end{bmatrix}^T = \begin{vmatrix} \vec{i} & \vec{j} & \vec{k} \\ F_{11} & F_{21} & F_{31} \\ F_{12} & F_{22} & F_{32} \end{vmatrix} = \begin{bmatrix} F_{21} \cdot F_{32} - F_{22} \cdot F_{31} \\ F_{12} \cdot F_{31} - F_{11} \cdot F_{32} \\ F_{11} \cdot F_{22} - F_{12} \cdot F_{21} \end{bmatrix}^T,$$

where \vec{i} , \vec{j} and \vec{k} are versors. According to this definition, we have $|\vec{n}| = 1$, $\vec{F}_1 \circ \vec{n} = 0$, and $\vec{F}_2 \circ \vec{n} = 0$. For \vec{F}_1 , \vec{F}_2 and \vec{n} , the following theorem is true:

Theorem 1. $\vec{F}_1 = \vec{F}_2 \times \vec{n}$ and $\vec{F}_2 = \vec{n} \times \vec{F}_1$.

Proof.

$$\begin{aligned} \vec{F}_1 &= \vec{F}_2 \times \vec{n} = \begin{vmatrix} \vec{i} & \vec{j} & \vec{k} \\ F_{12} & F_{22} & F_{32} \\ n_1 & n_2 & n_3 \end{vmatrix} \stackrel{\text{Eq. 1}}{=} \\ &= \begin{bmatrix} F_{22}(F_{11}F_{22} - F_{21}F_{12}) - F_{32}(F_{31}F_{12} - F_{11}F_{32}) \\ F_{32}(F_{21}F_{32} - F_{31}F_{22}) - F_{12}(F_{11}F_{22} - F_{21}F_{12}) \\ F_{12}(F_{31}F_{12} - F_{11}F_{32}) - F_{22}(F_{21}F_{32} - F_{31}F_{22}) \end{bmatrix}^T = \\ &= \begin{bmatrix} F_{22}^2F_{11} - F_{21}F_{12}F_{22} - F_{31}F_{32}F_{12} + F_{11}F_{32}^2 \\ F_{32}^2F_{21} - F_{31}F_{32}F_{22} - F_{11}F_{12}F_{22} + F_{21}F_{12}^2 \\ F_{12}^2F_{31} - F_{11}F_{12}F_{32} - F_{21}F_{22}F_{32} + F_{31}F_{22}^2 \end{bmatrix}^T = \\ &= \begin{bmatrix} F_{11}(F_{22}^2 + F_{32}^2) - F_{12}(F_{21}F_{22} + F_{31}F_{32}) \\ F_{21}(F_{12}^2 + F_{32}^2) - F_{22}(F_{31}F_{32} + F_{11}F_{12}) \\ F_{31}(F_{12}^2 + F_{22}^2) - F_{32}(F_{11}F_{12} + F_{21}F_{22}) \end{bmatrix}^T \stackrel{\text{Eq. 2}}{=} \\ &= \begin{bmatrix} F_{11}(F_{22}^2 + F_{32}^2) + F_{12}F_{11}F_{12} \\ F_{21}(F_{12}^2 + F_{32}^2) + F_{22}F_{21}F_{22} \\ F_{31}(F_{12}^2 + F_{22}^2) + F_{32}F_{31}F_{32} \end{bmatrix}^T \stackrel{\text{Eq. 1}}{=} \begin{bmatrix} F_{11} \\ F_{21} \\ F_{31} \end{bmatrix}^T = \vec{F}_1. \end{aligned}$$

The second proof is analogous. □

Remark 1. According to Theorem 1, the following formulas hold:

$$\begin{cases} F_{11} = F_{22}n_3 - F_{32}n_2 \\ F_{21} = F_{32}n_1 - F_{12}n_3 \\ F_{31} = F_{12}n_2 - F_{22}n_1 \end{cases} \quad (4)$$

$$\begin{cases} F_{12} = F_{31}n_2 - F_{21}n_3 \\ F_{22} = F_{11}n_3 - F_{31}n_1 \\ F_{32} = F_{21}n_1 - F_{11}n_2 \end{cases} \quad (5)$$

Additionally, we can proof the following:

Theorem 2. *The inverse matrix of*

$$\mathcal{R} = \begin{bmatrix} F_{11} & F_{12} & n_1 & 0 \\ F_{21} & F_{22} & n_2 & 0 \\ F_{31} & F_{32} & n_3 & 0 \\ 0 & 0 & 0 & 1 \end{bmatrix}$$

constructed from \vec{F}_1, \vec{F}_2 and \vec{n} can be expressed as:

$$\mathcal{R}^{-1} = \begin{bmatrix} F_{11} & F_{21} & F_{31} & 0 \\ F_{12} & F_{22} & F_{32} & 0 \\ n_1 & n_2 & n_3 & 0 \\ 0 & 0 & 0 & 1 \end{bmatrix}.$$

Proof. The determinant of the \mathcal{R} matrix is:

$$\begin{aligned} \det \mathcal{R} &= F_{11}(F_{22}n_3 - F_{32}n_2) + F_{21}(F_{32}n_1 - F_{12}n_3) + F_{31}(F_{12}n_2 - F_{22}n_1) \stackrel{\text{Eq. 4}}{=} \\ &= F_{11}^2 + F_{21}^2 + F_{31}^2 \stackrel{\text{Eq. 1}}{=} 1 \end{aligned} \tag{6}$$

Let us calculate the cofactor matrix \mathcal{R}^D :

$$\begin{aligned} \mathcal{R}^D &= \begin{bmatrix} F_{22}n_3 - F_{32}n_2 & F_{31}n_2 - F_{21}n_3 & F_{21}F_{32} - F_{31}F_{22} & 0 \\ F_{32}n_1 - F_{12}n_3 & F_{11}n_3 - F_{31}n_1 & F_{31}F_{12} - F_{11}F_{32} & 0 \\ F_{12}n_2 - F_{22}n_1 & F_{21}n_1 - F_{11}n_2 & F_{11}F_{22} - F_{21}F_{12} & 0 \\ 0 & 0 & 0 & \det \mathcal{R} \end{bmatrix} \stackrel{\text{Eq. 4, 5, 1}}{=} \\ &= \begin{bmatrix} F_{11} & F_{12} & n_1 & 0 \\ F_{21} & F_{22} & n_2 & 0 \\ F_{31} & F_{32} & n_3 & 0 \\ 0 & 0 & 0 & 1 \end{bmatrix}. \end{aligned}$$

Therefore—by the definition of the inverse matrix—we have:

$$\mathcal{R}^{-1} = \frac{1}{\det \mathcal{R}} (\mathcal{R}^D)^T = \begin{bmatrix} F_{11} & F_{21} & F_{31} & 0 \\ F_{12} & F_{22} & F_{32} & 0 \\ n_1 & n_2 & n_3 & 0 \\ 0 & 0 & 0 & 1 \end{bmatrix}. \tag{7}$$

□

3 TRANSFERRING ROIS ACROSS MODALITIES

In this section, we derive the formulas for transferring ROIs across different modalities. We exploit

the expressions presented and proven in the previous section, as well as the image information which can be extracted from each DICOM file¹. The derived equations are *independent* from the underlying modality, and can be easily applied to process any pair of modalities side-by-side.

Let

$$\begin{bmatrix} P_x \\ P_y \\ P_z \\ 1 \end{bmatrix} = \begin{bmatrix} F_{11}\Delta r & F_{12}\Delta c & n_1\Delta s & S_x \\ F_{21}\Delta r & F_{22}\Delta c & n_2\Delta s & S_y \\ F_{31}\Delta r & F_{32}\Delta c & n_3\Delta s & S_z \\ 0 & 0 & 0 & 1 \end{bmatrix} \begin{bmatrix} r \\ c \\ s \\ 1 \end{bmatrix} = \mathcal{A} \begin{bmatrix} r \\ c \\ s \\ 1 \end{bmatrix}, \tag{8}$$

where:

- P_{xyz} —Coordinates of the voxel (c, r) in the image plane (in mm).
- S_{xyz} —Image position (0020, 0032 DICOM attribute). It is the location from the origin (in mm).

¹For more details see: http://nipy.org/nibabel/dicom/dicom_orientation.html; last access date: Oct. 9, 2017.

- $F_{:,1}, F_{:,2}$ —Column (Y) and row (X) direction cosine of the image orientation (0020, 0037 DICOM attribute). These vectors are normal, and $F_{:,1} \circ F_{:,2} = 0$.
- r —Row index to the image plane. The first row index is zero.
- Δr , where $\Delta r \neq 0$ —Row pixel resolution of the pixel spacing (0028, 0030 DICOM attribute) (in mm).
- c —Column index to the image plane. The first column index is zero.
- Δc , where $\Delta c \neq 0$ —Column pixel resolution of the pixel spacing (0028, 0030 DICOM attribute) (in mm).
- s —Slice index to the slice plane. The first slice index is zero.
- Δs , where $\Delta s \neq 0$ —Spacing between the consecutive slices (in mm).
- n_i , where $i \in \{1, 2, 3\}$ —Vector orthogonal to $F_{:,1}$ and $F_{:,2}$.

Taking into account the definition of \vec{n} (see Eq. 3 and Def. 1, especially Eq. 1), the determinant of the \mathcal{A} matrix becomes:

$$\begin{aligned} \det \mathcal{A} &= \begin{vmatrix} F_{11}\Delta r & F_{12}\Delta c & n_1\Delta s & S_x \\ F_{21}\Delta r & F_{22}\Delta c & n_2\Delta s & S_y \\ F_{31}\Delta r & F_{32}\Delta c & n_3\Delta s & S_z \\ 0 & 0 & 0 & 1 \end{vmatrix} = \\ &= \Delta r\Delta c\Delta s \cdot \begin{vmatrix} F_{11} & F_{12} & n_1 & 0 \\ F_{21} & F_{22} & n_2 & 0 \\ F_{31} & F_{32} & n_3 & 0 \\ 0 & 0 & 0 & 1 \end{vmatrix} \stackrel{\text{Eq. 6}}{=} \Delta r\Delta c\Delta s \cdot 1 \neq 0. \end{aligned}$$

Consider the following decomposition of the \mathcal{A} matrix into the translation, rotation and scaling matrices:

$$\mathcal{A} = \mathcal{T} \cdot \mathcal{R} \cdot \mathcal{S}, \tag{9}$$

$$\tag{10}$$

where

$$\mathcal{T} = \begin{bmatrix} 1 & 0 & 0 & S_x \\ 0 & 1 & 0 & S_y \\ 0 & 0 & 1 & S_z \\ 0 & 0 & 0 & 1 \end{bmatrix}, \mathcal{R} = \begin{bmatrix} F_{11} & F_{12} & n_1 & 0 \\ F_{21} & F_{22} & n_2 & 0 \\ F_{31} & F_{32} & n_3 & 0 \\ 0 & 0 & 0 & 1 \end{bmatrix}, \mathcal{S} = \begin{bmatrix} \Delta r & 0 & 0 & 0 \\ 0 & \Delta c & 0 & 0 \\ 0 & 0 & \Delta s & 0 \\ 0 & 0 & 0 & 1 \end{bmatrix}. \tag{11}$$

Let us multiply the right side of Eq. 9:

$$\begin{aligned} \mathcal{T} \cdot \mathcal{R} \cdot \mathcal{S} &= \begin{bmatrix} 1 & 0 & 0 & S_x \\ 0 & 1 & 0 & S_y \\ 0 & 0 & 1 & S_z \\ 0 & 0 & 0 & 1 \end{bmatrix} \begin{bmatrix} F_{11} & F_{12} & n_1 & 0 \\ F_{21} & F_{22} & n_2 & 0 \\ F_{31} & F_{32} & n_3 & 0 \\ 0 & 0 & 0 & 1 \end{bmatrix} \begin{bmatrix} \Delta r & 0 & 0 & 0 \\ 0 & \Delta c & 0 & 0 \\ 0 & 0 & \Delta s & 0 \\ 0 & 0 & 0 & 1 \end{bmatrix} = \\ &= \begin{bmatrix} 1 & 0 & 0 & S_x \\ 0 & 1 & 0 & S_y \\ 0 & 0 & 1 & S_z \\ 0 & 0 & 0 & 1 \end{bmatrix} \begin{bmatrix} F_{11}\Delta r & F_{12}\Delta c & n_1\Delta s & 0 \\ F_{21}\Delta r & F_{22}\Delta c & n_2\Delta s & 0 \\ F_{31}\Delta r & F_{32}\Delta c & n_3\Delta s & 0 \\ 0 & 0 & 0 & 1 \end{bmatrix} = \\ &= \begin{bmatrix} F_{11}\Delta r & F_{12}\Delta c & n_1\Delta s & S_x \\ F_{21}\Delta r & F_{22}\Delta c & n_2\Delta s & S_y \\ F_{31}\Delta r & F_{32}\Delta c & n_3\Delta s & S_z \\ 0 & 0 & 0 & 1 \end{bmatrix} = \mathcal{A} \end{aligned}$$

Such decomposition helps find the inverse matrix of \mathcal{A} .

Remark 2. Since $\det \mathcal{A} = \Delta r\Delta c\Delta s \neq 0$, \mathcal{T} , \mathcal{R} and \mathcal{S} are invertible (Theorem 2):

$$\mathcal{T}^{-1} = \begin{bmatrix} 1 & 0 & 0 & -S_x \\ 0 & 1 & 0 & -S_y \\ 0 & 0 & 1 & -S_z \\ 0 & 0 & 0 & 1 \end{bmatrix}, \mathcal{R}^{-1} = \begin{bmatrix} F_{11} & F_{21} & F_{31} & 0 \\ F_{12} & F_{22} & F_{32} & 0 \\ n_1 & n_2 & n_3 & 0 \\ 0 & 0 & 0 & 1 \end{bmatrix}, \mathcal{S}^{-1} = \begin{bmatrix} \frac{1}{\Delta r} & 0 & 0 & 0 \\ 0 & \frac{1}{\Delta c} & 0 & 0 \\ 0 & 0 & \frac{1}{\Delta s} & 0 \\ 0 & 0 & 0 & 1 \end{bmatrix}. \tag{12}$$

In order to transfer ROIs across images, P_{xyz} values (in Eq. 8) should be the same for both of them (the d and s subscripts denote the destination and source image, respectively). Therefore, we get:

$$\begin{bmatrix} P_x \\ P_y \\ P_z \\ 1 \end{bmatrix} = \mathcal{A}_s \cdot \mathcal{V}_s = \begin{bmatrix} F_{11}^s \Delta r_s & F_{12}^s \Delta c_s & n_1^s \Delta s_s & S_x^s \\ F_{21}^s \Delta r_s & F_{22}^s \Delta c_s & n_2^s \Delta s_s & S_y^s \\ F_{31}^s \Delta r_s & F_{32}^s \Delta c_s & n_3^s \Delta s_s & S_z^s \\ 0 & 0 & 0 & 1 \end{bmatrix} \begin{bmatrix} r_s \\ c_s \\ s_s \\ 1 \end{bmatrix}$$

$$\begin{bmatrix} P_x \\ P_y \\ P_z \\ 1 \end{bmatrix} = \mathcal{A}_d \cdot \mathcal{V}_d = \begin{bmatrix} F_{11}^d \Delta r_d & F_{12}^d \Delta c_d & n_1^d \Delta s_d & S_x^d \\ F_{21}^d \Delta r_d & F_{22}^d \Delta c_d & n_2^d \Delta s_d & S_y^d \\ F_{31}^d \Delta r_d & F_{32}^d \Delta c_d & n_3^d \Delta s_d & S_z^d \\ 0 & 0 & 0 & 1 \end{bmatrix} \begin{bmatrix} r_d \\ c_d \\ s_d \\ 1_d \end{bmatrix}$$

Then:

$$\mathcal{T}_s \cdot \mathcal{R}_s \cdot \mathcal{S}_s \cdot \mathcal{V}_s = \mathcal{T}_d \cdot \mathcal{R}_d \cdot \mathcal{S}_d \cdot \mathcal{V}_d \quad |\rightarrow \mathcal{T}_d^{-1} \quad (13)$$

$$\mathcal{T}_d^{-1} \cdot \mathcal{T}_s \cdot \mathcal{R}_s \cdot \mathcal{S}_s \cdot \mathcal{V}_s = \mathcal{R}_d \cdot \mathcal{S}_d \cdot \mathcal{V}_d \quad |\rightarrow \mathcal{R}_d^{-1} \quad (14)$$

$$\mathcal{R}_d^{-1} \cdot \mathcal{T}_d^{-1} \cdot \mathcal{T}_s \cdot \mathcal{R}_s \cdot \mathcal{S}_s \cdot \mathcal{V}_s = \mathcal{S}_d \cdot \mathcal{V}_d \quad |\rightarrow \mathcal{S}_d^{-1} \quad (15)$$

$$\mathcal{S}_d^{-1} \cdot \mathcal{R}_d^{-1} \cdot \mathcal{T}_d^{-1} \cdot \mathcal{T}_s \cdot \mathcal{R}_s \cdot \mathcal{S}_s \cdot \mathcal{V}_s = \mathcal{V}_d \quad (16)$$

$$(\mathcal{S}_d^{-1} \cdot \mathcal{R}_d^{-1}) \cdot (\mathcal{T}_d^{-1} \cdot \mathcal{A}_s) \cdot \mathcal{V}_s = \mathcal{V}_d \quad (17)$$

$$\mathcal{V}_d = \mathcal{A}_d^{-1} \cdot \mathcal{A}_s \cdot \mathcal{V}_s \quad (18)$$

Let us continue with Eq. 17:

$$(\mathcal{S}_d^{-1} \cdot \mathcal{R}_d^{-1}) = \begin{bmatrix} \frac{1}{\Delta r_d} & 0 & 0 & 0 \\ 0 & \frac{1}{\Delta c_d} & 0 & 0 \\ 0 & 0 & \frac{1}{\Delta s_d} & 0 \\ 0 & 0 & 0 & 1 \end{bmatrix} \cdot \begin{bmatrix} F_{11}^d & F_{21}^d & F_{31}^d & 0 \\ F_{12}^d & F_{22}^d & F_{32}^d & 0 \\ n_1^d & n_2^d & n_3^d & 0 \\ 0 & 0 & 0 & 1 \end{bmatrix} \Rightarrow$$

$$(\mathcal{S}_d^{-1} \cdot \mathcal{R}_d^{-1}) = \begin{bmatrix} \frac{1}{\Delta r_d} F_{11}^d & \frac{1}{\Delta r_d} F_{21}^d & \frac{1}{\Delta r_d} F_{31}^d & 0 \\ \frac{1}{\Delta c_d} F_{12}^d & \frac{1}{\Delta c_d} F_{22}^d & \frac{1}{\Delta c_d} F_{32}^d & 0 \\ \frac{1}{\Delta s_d} n_1^d & \frac{1}{\Delta s_d} n_2^d & \frac{1}{\Delta s_d} n_3^d & 0 \\ 0 & 0 & 0 & 1 \end{bmatrix} \quad (19)$$

$$(\mathcal{T}_d^{-1} \cdot \mathcal{A}_s) = \begin{bmatrix} 1 & 0 & 0 & -S_x^d \\ 0 & 1 & 0 & -S_y^d \\ 0 & 0 & 1 & -S_z^d \\ 0 & 0 & 0 & 1 \end{bmatrix} \cdot \begin{bmatrix} \Delta r_s F_{11}^s & \Delta c_s F_{12}^s & \Delta s_s n_1^s & S_x^s \\ \Delta r_s F_{21}^s & \Delta c_s F_{22}^s & \Delta s_s n_2^s & S_y^s \\ \Delta r_s F_{31}^s & \Delta c_s F_{32}^s & \Delta s_s n_3^s & S_z^s \\ 0 & 0 & 0 & 1 \end{bmatrix} \Rightarrow$$

$$(\mathcal{T}_d^{-1} \cdot \mathcal{A}_s) = \begin{bmatrix} F_{11}^s \Delta r_s & F_{12}^s \Delta c_s & n_1^s \Delta s_s & S_x^s - S_x^d \\ F_{21}^s \Delta r_s & F_{22}^s \Delta c_s & n_2^s \Delta s_s & S_y^s - S_y^d \\ F_{31}^s \Delta r_s & F_{32}^s \Delta c_s & n_3^s \Delta s_s & S_z^s - S_z^d \\ 0 & 0 & 0 & 1 \end{bmatrix} \quad (20)$$

Let us introduce the vector \vec{D} , given as:

$$\vec{D} = \begin{bmatrix} D_x \\ D_y \\ D_z \end{bmatrix}^T = \begin{bmatrix} S_x^s - S_x^d \\ S_y^s - S_y^d \\ S_z^s - S_z^d \end{bmatrix} \quad (21)$$

and:

$$(\mathcal{T}_d^{-1} \cdot \mathcal{A}_s) = \begin{bmatrix} F_{11}^s \Delta r_s & F_{12}^s \Delta c_s & n_1^s \Delta s_s & D_x \\ F_{21}^s \Delta r_s & F_{22}^s \Delta c_s & n_2^s \Delta s_s & D_y \\ F_{31}^s \Delta r_s & F_{32}^s \Delta c_s & n_3^s \Delta s_s & D_z \\ 0 & 0 & 0 & 1 \end{bmatrix} \quad (22)$$

Combining Eq. 19 and Eq. 20, we obtain:

$$\mathcal{A}_d^{-1} \cdot \mathcal{A}_s = \begin{bmatrix} \frac{1}{\Delta r_d} F_{11}^d & \frac{1}{\Delta r_d} F_{21}^d & \frac{1}{\Delta r_d} F_{31}^d & 0 \\ \frac{1}{\Delta c_d} F_{12}^d & \frac{1}{\Delta c_d} F_{22}^d & \frac{1}{\Delta c_d} F_{32}^d & 0 \\ \frac{1}{\Delta s_d} n_1^d & \frac{1}{\Delta s_d} n_2^d & \frac{1}{\Delta s_d} n_3^d & 0 \\ 0 & 0 & 0 & 1 \end{bmatrix} \cdot \begin{bmatrix} F_{11}^s \Delta r_s & F_{12}^s \Delta c_s & n_1^s \Delta s_s & D_x \\ F_{21}^s \Delta r_s & F_{22}^s \Delta c_s & n_2^s \Delta s_s & D_y \\ F_{31}^s \Delta r_s & F_{32}^s \Delta c_s & n_3^s \Delta s_s & D_z \\ 0 & 0 & 0 & 1 \end{bmatrix} =$$

$$= \begin{bmatrix} \frac{\Delta r_s}{\Delta r_d} (F_{11}^d F_{11}^s + F_{21}^d F_{21}^s + F_{31}^d F_{31}^s) & \frac{\Delta c_s}{\Delta r_d} (F_{11}^d F_{12}^s + F_{21}^d F_{22}^s + F_{31}^d F_{32}^s) \\ \frac{\Delta r_s}{\Delta c_d} (F_{12}^d F_{11}^s + F_{22}^d F_{21}^s + F_{32}^d F_{31}^s) & \frac{\Delta c_s}{\Delta c_d} (F_{12}^d F_{12}^s + F_{22}^d F_{22}^s + F_{32}^d F_{32}^s) \\ \frac{\Delta r_s}{\Delta s_d} (n_1^d F_{11}^s + n_2^d F_{21}^s + n_3^d F_{31}^s) & \frac{\Delta c_s}{\Delta s_d} (n_1^d F_{12}^s + n_2^d F_{22}^s + n_3^d F_{32}^s) \\ 0 & 0 \\ \frac{\Delta s_s}{\Delta r_d} (F_{11}^d n_1^s + F_{21}^d n_2^s + F_{31}^d n_3^s) & \frac{1}{\Delta r_d} (F_{11}^d D_x + F_{21}^d D_y + F_{31}^d D_z) \\ \frac{\Delta s_s}{\Delta c_d} (F_{12}^d n_1^s + F_{22}^d n_2^s + F_{32}^d n_3^s) & \frac{1}{\Delta c_d} (F_{12}^d D_x + F_{22}^d D_y + F_{32}^d D_z) \\ \frac{\Delta s_s}{\Delta s_d} (n_1^d n_1^s + n_2^d n_2^s + n_3^d n_3^s) & \frac{1}{\Delta s_d} (n_1^d D_x + n_2^d D_y + n_3^d D_z) \\ 0 & 1 \end{bmatrix}$$

From the definition of the dot product, we get:

$$\mathcal{A}_d^{-1} \cdot \mathcal{A}_s = \begin{bmatrix} \frac{\Delta r_s}{\Delta r_d} (\vec{F}_1^d \circ \vec{F}_1^s) & \frac{\Delta c_s}{\Delta r_d} (\vec{F}_1^d \circ \vec{F}_2^s) & \frac{\Delta s_s}{\Delta r_d} (\vec{F}_1^d \circ \vec{n}_s) & \frac{1}{\Delta r_d} \vec{F}_1^d \circ \vec{D} \\ \frac{\Delta r_s}{\Delta c_d} (\vec{F}_2^d \circ \vec{F}_1^s) & \frac{\Delta c_s}{\Delta c_d} (\vec{F}_2^d \circ \vec{F}_2^s) & \frac{\Delta s_s}{\Delta c_d} (\vec{F}_2^d \circ \vec{n}_s) & \frac{1}{\Delta c_d} \vec{F}_2^d \circ \vec{D} \\ \frac{\Delta r_s}{\Delta s_d} (\vec{n}_d \circ \vec{F}_1^s) & \frac{\Delta c_s}{\Delta s_d} (\vec{n}_d \circ \vec{F}_2^s) & \frac{\Delta s_s}{\Delta s_d} (\vec{n}_d \circ \vec{n}_s) & \frac{1}{\Delta s_d} (\vec{n}_d \circ \vec{D}) \\ 0 & 0 & 0 & 1 \end{bmatrix}$$

Using Eq. 18 gives:

$$\mathcal{V}_d = \begin{bmatrix} r_d \\ c_d \\ s_d \\ 1 \end{bmatrix} = \mathcal{A}_d^{-1} \cdot \mathcal{A}_s \cdot \mathcal{V}_s =$$

$$= \begin{bmatrix} \frac{\Delta r_s}{\Delta r_d} (\vec{F}_1^d \circ \vec{F}_1^s) & \frac{\Delta c_s}{\Delta r_d} (\vec{F}_1^d \circ \vec{F}_2^s) & \frac{\Delta s_s}{\Delta r_d} (\vec{F}_1^d \circ \vec{n}_s) & \frac{1}{\Delta r_d} \vec{F}_1^d \circ \vec{D} \\ \frac{\Delta r_s}{\Delta c_d} (\vec{F}_2^d \circ \vec{F}_1^s) & \frac{\Delta c_s}{\Delta c_d} (\vec{F}_2^d \circ \vec{F}_2^s) & \frac{\Delta s_s}{\Delta c_d} (\vec{F}_2^d \circ \vec{n}_s) & \frac{1}{\Delta c_d} (\vec{F}_2^d \circ \vec{D}) \\ \frac{\Delta r_s}{\Delta s_d} (\vec{n}_d \circ \vec{F}_1^s) & \frac{\Delta c_s}{\Delta s_d} (\vec{n}_d \circ \vec{F}_2^s) & \frac{\Delta s_s}{\Delta s_d} (\vec{n}_d \circ \vec{n}_s) & \frac{1}{\Delta s_d} (\vec{n}_d \circ \vec{D}) \\ 0 & 0 & 0 & 1 \end{bmatrix} \begin{bmatrix} r_s \\ c_s \\ s_s \\ 1 \end{bmatrix}$$

Finally, we have:

$$\begin{cases} r_d = \frac{1}{\Delta r_d} (\Delta r_s r_s (\vec{F}_1^d \circ \vec{F}_1^s) + \Delta c_s c_s (\vec{F}_1^d \circ \vec{F}_2^s) + \Delta s_s s_s (\vec{F}_1^d \circ \vec{n}_s) + (\vec{F}_1^d \circ \vec{D})) \\ c_d = \frac{1}{\Delta c_d} (\Delta r_s r_s (\vec{F}_2^d \circ \vec{F}_1^s) + \Delta c_s c_s (\vec{F}_2^d \circ \vec{F}_2^s) + \Delta s_s s_s (\vec{F}_2^d \circ \vec{n}_s) + (\vec{F}_2^d \circ \vec{D})) \\ s_d = \frac{1}{\Delta s_d} (\Delta r_s r_s (\vec{n}_d \circ \vec{F}_1^s) + \Delta c_s c_s (\vec{n}_d \circ \vec{F}_2^s) + \Delta s_s s_s (\vec{n}_d \circ \vec{n}_s) + (\vec{n}_d \circ \vec{D})) \end{cases} \quad (23)$$

Eq. 23 can be used to transfer the information (e.g., ROIs) across images.

4 CASE STUDY: PET/CT LUNG SEGMENTATION AND ANALYSIS

Lung cancer accounts for 12.7% of the world's total cancer incidence, and the PET/CT imaging plays a pivotal role in its diagnosis, staging and treatment, as it provides both anatomical and functional information about the patient. Therefore, automated PET/CT segmentation and analysis techniques attracted research attention and they are actively being developed (Mokri et al., 2012; Zhao et al., 2015). In our very recent work (Nalepa et al., 2016), we proposed an automated approach for PET/CT image analysis which does not require any user intervention. The experimental study (44 patients, age: 68.7 ± 10.3 years, 32 males who underwent FDG-PET/CT using GE Discovery; the clinical information was available for 42 patients: I: 1, II: 9, III: 28, and IV: 4) revealed that our automated histogram-based texture analysis (Miles et al., 2013) of filtered images² allowed for predicting survival (kurtosis, $p = .028$). Therefore, we showed that using quantitative techniques (CT texture analysis) in addition to existing measures, including size, density and glucose uptake, can enhance the diagnostic efficiency of PET/CT.

Algorithm 1: Hands-free PET/CT analysis algorithm.

- 1: Identify co-registered CT and PET series;
 - 2: Segment lungs in CT;
 - 3: Segment *hot-spots* in PET in the **lung range**;
 - 4: **Transfer hot-spot ROIs to CT**;
 - 5: Apply texture analysis algorithm in CT;
 - 6: Generate report;
-

The high-level pseudo-code of our hands-free PET/CT analysis algorithm is presented in Algorithm 1 (we boldfaced the steps which require transferring information between modalities). After identifying the co-registered CT and PET series (line 1), the CT frames are segmented in search of lungs (their base and apex). Then, the PET images are processed (line 3), *only* in the lung region (between base and apex). First, a threshold is extracted (40% of the global maximum pixel value, as suggested in (Win et al., 2013)). This threshold is used to identify hot-spots in

²We used our TexRAD software for texture analysis: <http://texrad.com/>.

PET images (connected regions exceeding this value). Hot-spots are transferred back to CT using Eq. 23 derived in Section 3 (line 4). In the last step, we apply the TexRAD algorithm (line 5), and generate a report (line 6) which is saved for review. TexRAD is a filtration-histogram approach to texture analysis which comprises image filtration performed to highlight image features of a specified size. This procedure is followed by the histogram analysis for quantification of derived features using various measures (e.g., kurtosis, skewness, standard deviation or entropy). Such texture features were shown to be correlated with various clinical parameters (Weiss et al., 2014; Parikh et al., 2014), not only in oncology (Rădulescu et al., 2014).

Example images generated at the most important steps of the processing pipeline are shown in Figure 1. The images are co-registered, and the CT frames are segmented to find lungs (Figure 1a). Additionally, in our approach the convex hulls of lungs are determined (those regions are larger compared with the segmented lungs), since the tumors may be associated with the lung wall or mediastinum. Then, the lung ROIs are transferred to PET (using Eq. 23) to find the location of lungs in PET series, and the hot-spots are segmented (Figure 1b). Afterwards, the hot-spot ROI is transferred back to the corresponding CT image (by location), and it undergoes the texture analysis at various spatial frequencies (scales). Finally, the extracted texture features, along with the filtered images are saved in reports and can be further investigated. This PET/CT analysis example shows how to efficiently exploit the information (functional and anatomical) about the patient exposed by two different modalities. The key part of this analysis is concerned with the possibility of transferring data (e.g., ROIs) across the co-registered images, as presented in Section 3. It is worth mentioning that the lung and hot-spot segmentation algorithms can be easily replaced with new, perhaps more efficient techniques without impacting the entire hands-free processing pipeline. For more details, see (Nalepa et al., 2016).

5 CONCLUSIONS

In this paper, we focused on the side-by-side analysis of multimodal medical images, and derived formulas which can be used to transfer information (e.g., ROIs) across different modalities. Since the formulas are generic, they can be very easily applied to any pair of co-registered images. Such multimodal analysis became crucial in the clinical practice because it enhances the diagnostic efficiency of this kind of imaging by cou-

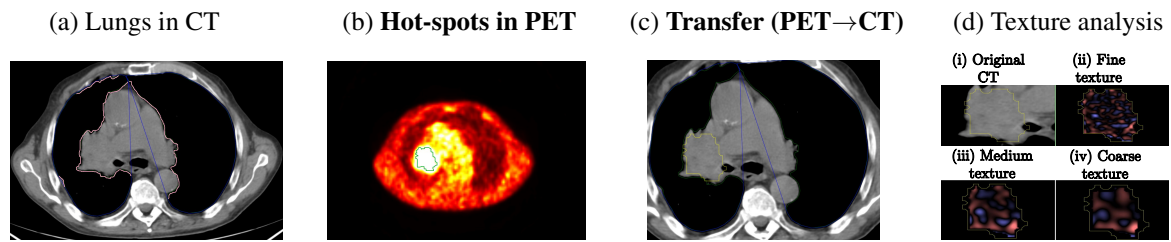


Figure 1: Example images generated at the most important steps of the PET/CT analysis: (a) lungs segmented in CT (light pink ROIs indicate lungs, whereas blue ROIs show their convex hulls), (b) hot-spot segmented in PET, (c) hot-spot transferred from PET to CT (annotated in yellow), and (d) texture analysis at various scales (fine, medium and coarse) using the TexRAD algorithm. We boldfaced the steps in which we benefit from transferring the information between two modalities.

pling complementary patient information (e.g., anatomical and functional). It leads to extracting new information about the patient condition and treatment response, which would not be revealed if the images were processed separately.

ACKNOWLEDGEMENTS

This research was supported by the National Centre for Research and Development under the Innomed Research and Development Grant No. POIR.01.02.00-00-0030/15.

REFERENCES

- Deregnacourt, T., Samir, C., and Yao, A.-F. (2016). A regression model for registering multimodal images. *Procedia Computer Science (MIUA 2016)*, 90:42–47.
- Estorch, M. and Carrio, I. (2013). Future challenges of multimodality imaging. In Schober, O. and Riemann, B., editors, *Mol. Imag. in Onc.*, pages 403–415, Heidelberg. Springer.
- Greulich, S. and Sechtem, U. (2015). Multimodality imaging in coronary artery disease – “the more the better?”. *Cor et Vasa*, 57(6):e462 – e469.
- Martí-Bonmatí, L., Sopena, R., Bartumeus, P., and Sopena, P. (2010). Multimodality imaging techniques. *Contrast Media & Molecular Imaging*, 5(4):180–189.
- Miles, K., Ganeshan, B., and Hayball, M. (2013). CT texture analysis using the filtration-histogram method: what do the measurements mean? *Canc. Im.*, 13(3):400–406.
- Mokri, S. S., Saripan, M. I., Marhaban, M. H., and Nordin, A. J. (2012). Lung segmentation in CT for thoracic PET-CT registration through visual study. In *Proc. IEEE-EMBS*, pages 550–554.
- Nalepa, J., Szymanek, J., Mcquaid, S., Endozo, R., Prakash, V., Ganeshan, B., Menys, A., Hayball, M. P., Ezhil, V., Bellamy, L., Crawshaw, J., Hall, J., Groves, A. M., and Nisbet, A. (2016). PET/CT in lung cancer: An automated imaging tool for decision support. In *Radiological Society of North America 2016 Scientific Assembly and Annual Meeting*, pages 1–2, Chicago IL, USA. RSNA.
- Parikh, J., Selmi, M., Charles-Edwards, G., Glendenning, J., Ganeshan, B., Verma, H., Mansi, J., Harries, M., Tutt, A., and Goh, V. (2014). Changes in primary breast cancer heterogeneity may augment midtreatment MR imaging assessment of response to neoadjuvant chemotherapy. *Radiology*, 272(1):100–112.
- Pichler, B. J., Judenhofer, M. S., and Pfannenber, C. (2008). Multimodal imaging approaches: PET/CT and PET/MRI. In Semmler, W. and Schwaiger, M., editors, *Molecular Imaging I*, pages 109–132, Heidelberg. Springer.
- Radulescu, E., Ganeshan, B., Shergill, S. S., Medford, N., Chatwin, C., Young, R. C., and Critchley, H. D. (2014). Grey-matter texture abnormalities and reduced hippocampal volume are distinguishing features of schizophrenia. *Psychiatry Research: Neuroimaging*, 223(3):179 – 186.
- Sui, J., Adali, T., Yu, Q., Chen, J., and Calhoun, V. D. (2012). A review of multivariate methods for multimodal fusion of brain data. *J. of Neurosc. Met.*, 204(1):68 – 81.
- Vandenberghe, S. and Marsden, P. K. (2015). PET-MRI: a review of challenges and solutions in the development of integrated multimodality imaging. *Physics in Medicine and Biology*, 60(4):R115.
- Weiss, G. J., Ganeshan, B., Miles, K. A., Campbell, D. H., Cheung, P. Y., Frank, S., and Korn, R. L. (2014). Noninvasive image texture analysis differentiates k-ras mutation from pan-wildtype nscl and is prognostic. *PLOS ONE*, 9(7):1–9.
- Win, T., Miles, K. A., Janes, S. M., Ganeshan, B., Shastry, M., Endozo, R., Meagher, M., Shortman, R. I., Wan, S., Kayani, I., Ell, P. J., and Groves, A. M. (2013). Tumor heterogeneity and permeability as measured on the ct component of PET/CT predict survival in patients with non-small cell lung cancer. *Clin. Cancer Res.*, 19(13):3591–3599.
- Zhao, J., Ji, G., Qiang, Y., Han, X., Pei, B., and Shi, Z. (2015). A new method of detecting pulmonary nodules with PET/CT based on an improved watershed algorithm. *PLOS ONE*, 10(4):1–15.